Vol. 04, Iss. 1 (2026) 29-42, DOI: 10.61552/JME.2026.01.003

Journal of Materials and Engineering

www.jme.aspur.rs

Research article

Experimental Investigation on the Performance Characteristics of SAE10W30 Lubricant Oil Blended with Nano-Additives

E. Sankar[a,*], K. Duraivelu[a]

[a]*Department of Mechanical Engineering, SRM Institute of Science and Technology, Kattankulathur, 603 203, India.*

Keywords:

Nano additives
Lubricant properties
Optimal mix
Factorial design
Taguchi method
Multi-objective polynomial program

* Corresponding author:

E. Sankar
E-mail: se1515@srmist.edu.in

Received: 20 November 2024
Revised: 27 December 2024
Accepted: 31 January 2025

A B S T R A C T

Nano additives are generally blended with the base lubricant oil, to enhance the lubricant characteristics. In this research, nano additives of SiO_2, Al_2O_3 and TiO_2 are blended with the base SAE10W30 oil with different proportions of mixture. 27 samples with three different levels of mix of nano additives are identified using factorial design of experiment. The experimental outcomes for the selected six characteristics of interest of specific wear rate, co-efficient of friction, kinematic viscosity, density, flash point and fire point are determined. Using Taguchi method, the optimal values for each property of lubricant are identified. Also, the optimal mix of all three nanoadditives is determined for all the desirable level of six properties of lubricant using multi-objective polynomial program in this research. The optimal mix is identified as 0.05 wt.% of SiO_2, 1 wt.% of TiO_2, and 0.3 wt.% of Al_2O_3.

1. INTRODUCTION

Conventional base oils, derived from refined crude oil, provide basic lubrication properties. Synthetic base oils, produced through chemical processes, offer superior performance with enhanced thermal stability, lower volatility, and better cold-temperature properties. Synthetic blends mix conventional and synthetic base oils to achieve a balance of performance and cost. The choice of base oil affects the overall performance of 10W-30 motor oil, influencing its viscosity stability, oxidation resistance, and ability to maintain protective lubrication under diverse temperature conditions.

Understanding the tribology of SAE10W-30 oils focused on friction, wear, and lubrication is essential for evaluating its performance in internal combustion engines. This multigrade oil

is designed to offer balanced viscosity characteristics, ensuring effective lubrication across a broad temperature range. At low temperatures, the oil remains fluid, reducing friction during engine startup, while at high temperatures, it retains sufficient thickness to protect engine components from wear. The oil's additives, including anti-wear agents, friction modifiers, and antioxidants, play critical roles in minimizing metal-to-metal contact, reducing oxidative degradation, and ensuring a stable lubricating film. This comprehensive tribological performance helps enhance engine efficiency, reduce fuel consumption, and extend engine life by minimizing friction and wear under varying operational conditions.

Society of Automotive Engineers (SAE) developed a grading system to classify motor oils based on their viscosity properties. SAE 10W-30 is a widely used multigrade motor oil in automotive and various engine applications. The "10W-30" designation provides specific information about the oil's viscosity at different temperatures, ensuring that it performs well under various operating conditions. SAE10W30 is a multi-grade engine oil with moderate viscosity, offering balanced performance in friction reduction and wear protection under varying temperatures and load conditions. Viscosity and grading are critical factors in determining the flow characteristics and classification of fluids, especially in motor oils like SAE 10W-30. Viscosity refers to a fluid's resistance to flow, with motor oil ensuring proper lubrication, cooling, and engine protection. SAE 10W-30, a multigrade oil, is designed to perform well across varying temperatures, with "10W" indicating cold-weather performance and "30" ensuring adequate viscosity at high operating temperatures. This oil provides reliable protection, reducing wear, improving fuel efficiency, and preventing deposits and sludge buildup. It is widely used in passenger cars, light trucks, small engines, marine engines, and even aircraft, offering consistent performance and lubrication across diverse applications.

2. METHODOLOGY

SAE 10W-30 is a versatile and dependable motor oil that delivers strong performance across a broad temperature range. Its multigrade formulation ensures effective lubrication and protection of engine components during cold starts and high-temperature operations. With advantages like enhanced fuel efficiency, superior engine protection, and effective deposit control, it is a popular choice for numerous automotive and engine applications. By understanding the characteristics and advantages of this oil, users can ensure optimal performance and longevity of their engines. SAE10W30 lubricant oil physical properties are listed in the Table 1.

Table 1. Physical properties of SAE 10W30 oil.

Physical properties	Test Method	Value
Kinematic Viscosity, cSt at 40°C	ASTM D-445	65.5
Kinematic Viscosity, cSt at 100°C	ASTM D-445	10.4
Viscosity Index	calculated	147
Pour Point, °C	ASTM D-97	-36
Sulfated Ash, Wt %	ASTM D-874	0.9
Phosphorus, Wt %	ASTM D-4981	0.077

Overall, this SAE 10W-30 lubricant is designed to offer balanced performance across a broad range of conditions, making it a reliable choice for engines requiring consistent protection and efficiency. Lubricant additives enhance base oils by reducing friction, minimizing wear, preventing oxidation and corrosion, and dispersing contaminants, ensuring optimal performance and machinery protection [1]. SiO_2 nanoparticles improve lubrication by forming a durable tribological layer that reduces friction and wear, extending component lifespan [2-3]. Their high surface area, chemical stability, and thermal resistance ensure effectiveness in demanding conditions. With optimized particle sizes, they balance anti-wear and friction reduction, making them ideal for enhancing lubricant performance [4-5]. Al_2O_3 nanoparticles enhance lubricants by reducing friction, improving wear resistance, and increasing thermal stability and load-carrying capacity. Their chemical stability prevents negative interactions, ensuring long-term effectiveness. Widely used in automotive, heavy-duty, aerospace, and marine applications, they boost fuel efficiency, extend equipment life, and provide reliable performance under extreme conditions. TiO_2 nanoparticles enhance lubricants by reducing friction, minimizing abrasive wear,

and forming protective tribo-films that extend machinery life. Their thermal stability and improved heat dissipation prevent overheating, while anti-corrosive properties protect metal surfaces from oxidation. Additionally, their photocatalytic nature helps decompose organic contaminants, keeping lubricants cleaner and more effective over time. The different characteristics of silicon dioxide are outlined in Table 2.

Table 2. Properties of additives.

Properties	SiO_2	TiO_2	Al_2O_3
Crystal structure	Amorphous	Polymorph	White Crystalline Powder
Atomic weight (g/mole)	60.08	79.87	101.96
Density (thermal, dry/ wet) g/cm^3	2.27	4.23	3.97
Molecules /cm^3	2.3x10^{22}	1.25x 10^{16}	9.8x 10^{18}
Specific Heat (J/g-K)	1.0	683	451
Melting Point °C	1700	1843	2072
Thermal Expansion Coefficient K^{-1}	5.6x10^{-7}	313 x 10^{-6}	12.66 x 10^{-6}
Young's Modulus N/m^2	6.6x10^{10}	29.3x 10^{10}	3.7x10^{10}
Poisson's Ratio	0.17	0.27	0.21
Thermal Conductivity W/m-K	1.1 - 1.4	7.09 -8.4	28 - 35
Relative Dielectric Constant	3.7-3.9	63.7	9.0 - 10.1

High-Resolution Scanning Electron Microscopy (HRSEM) is an advanced imaging technique that provides detailed and high-magnification images of the surfaces and structures of materials HRSEM is a powerful tool for analysing the microstructure and surface morphology of materials at the nanometer scale. Its high resolution, surface sensitivity, and versatility make it invaluable in material science, nanotechnology, biology, electronics, and tribology. By providing detailed and high-quality images, HRSEM aids in advancing our understanding of materials and their properties, leading to innovations and improvements across various fields.

Figure 1 shows the SEM image depicting SiO_2 nanoparticles with sizes ranging from approximately 71.42 nm to 106.0 nm, magnified 120,000 times. The nanoparticles, measured using an Everhart-Thornley Detector (ETD) at a high voltage of 20.00 kV, exhibit an irregular morphology, clustering together in various shapes and sizes. Figure 2 shows the Transmission electron microscopy (TEM) image of SiO_2 nanoparticles with a range of particle sizes with measurements labelled in nanometers, indicating diameters approximately 44.7 nm.

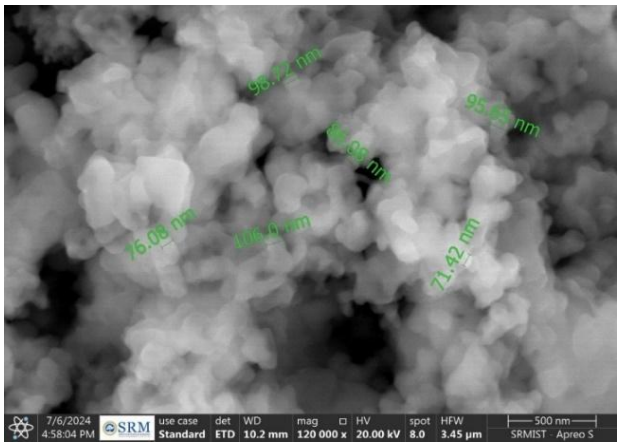

Fig. 1. SEM image of SiO_2.

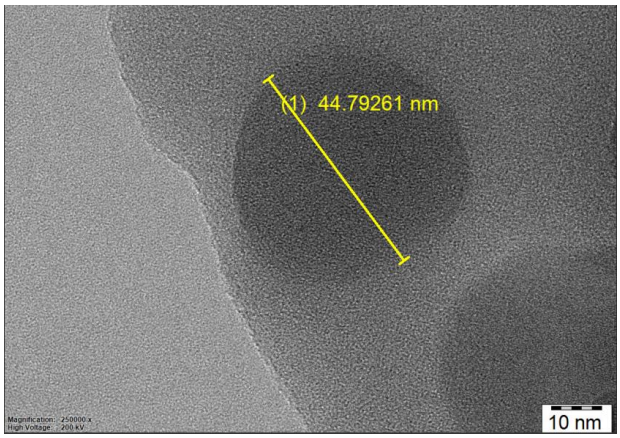

Fig. 2. TEM image of SiO_2.

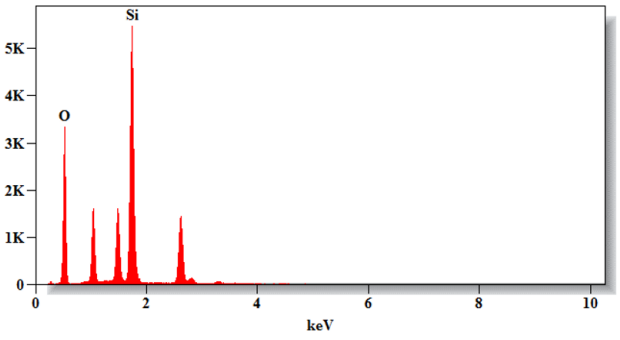

Fig. 3. Energy-dispersive X-ray spectroscopy.

Figure 3 shows the EDS spectrum of SiO_2 nanoparticles, confirming their composition with prominent silicon (~1.74 keV) and oxygen (~0.5 keV) peaks. The higher silicon peak intensity indicates a greater relative concentration, while the absence of other significant peaks suggests high sample purity. Quantitative analysis can further determine the exact element percentages.

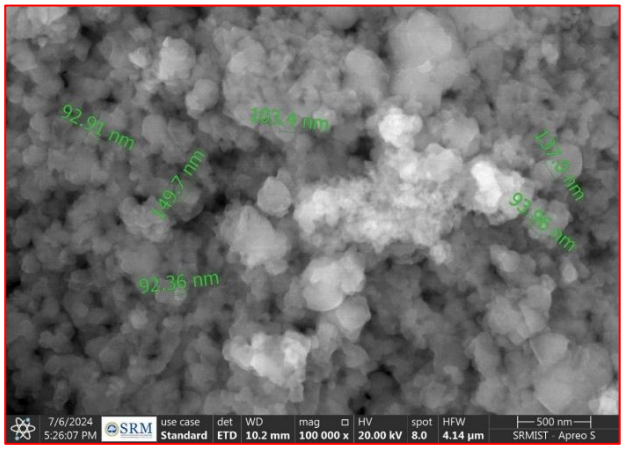

Fig. 4. SEM image of Al_2O_3.

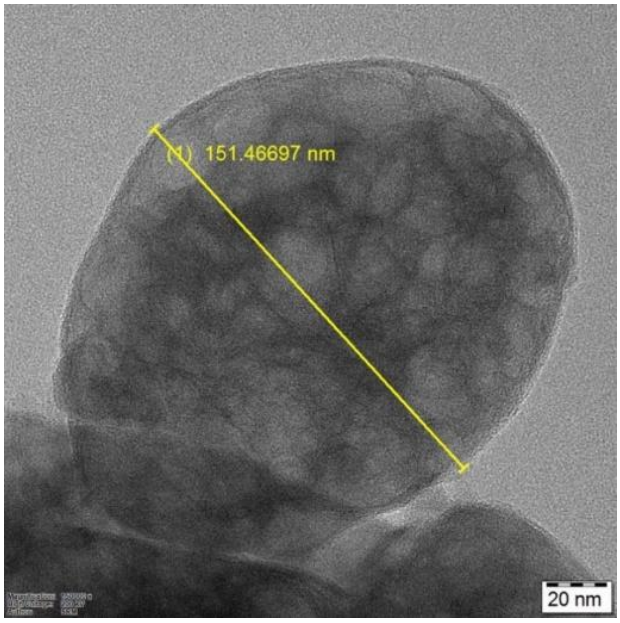

Fig. 5. TEM image of Al_2O_3.

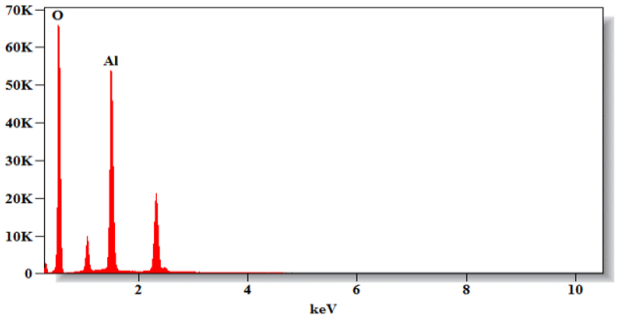

Fig. 6. Energy-dispersive X-ray spectroscopy (EDS)

Figures 4 and 5 show SEM and TEM images of Al_2O_3 nanoparticles, respectively, revealing particle sizes ranging from 92.36 nm to 151.4 nm, with detailed surface morphology at high magnifications. The working distance is 10.2 mm, and the horizontal field width is 4.14 µm, contributing to the high resolution and depth of field in the image. The nanoparticles appear to be agglomerated, forming clusters of various shapes and sizes. The scale bar at the bottom right, representing 500 nm, serves as a reference for the size of the particles. Figure 6 shows EDS spectrum of Al_2O_3 nanoparticles, showcasing characteristic peaks corresponding to the elements present in the sample. The prominent peaks at around 0.5 keV and 1.5 keV indicate the presence of oxygen (O) and aluminum (Al), respectively, which are the primary components of Al_2O_3. The intensity of these peaks suggests a significant concentration of both elements, confirming the successful synthesis of alumina nanoparticles. The absence of other major peaks implies that the sample is relatively pure, with minimal impurities, which is crucial for applications requiring high-purity materials.

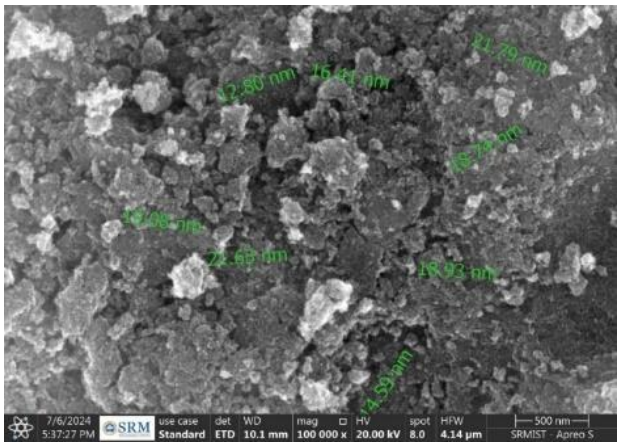

Fig. 7. SEM image of TiO_2.

Figure 7 shows a SEM image of TiO_2 nanoparticles, ranging from ~12.80 nm to 21.79 nm, with rough, irregular, and slightly agglomerated surfaces, captured at 100,000x magnification, highlighting their nanoscale features and potential applications. Figure 8 shows the TEM image of TiO_2 nanoparticles with a range of particle sizes with measurements labelled in nanometers, indicating diameters from approximately 6.3 nm to 9.68 nm. The image is captured at a magnification of 20 nm, using HRTEM providing a detailed view of the nanoparticles' surface morphology. Figure 9

shows EDS spectrum of TiO_2 nanoparticles revealing distinct peaks corresponding to titanium (Ti) and oxygen (O), the primary elements in the sample. The significant peaks at around 0.5 keV for oxygen and at approximately 4.5 keV for titanium confirm the successful synthesis of TiO_2.

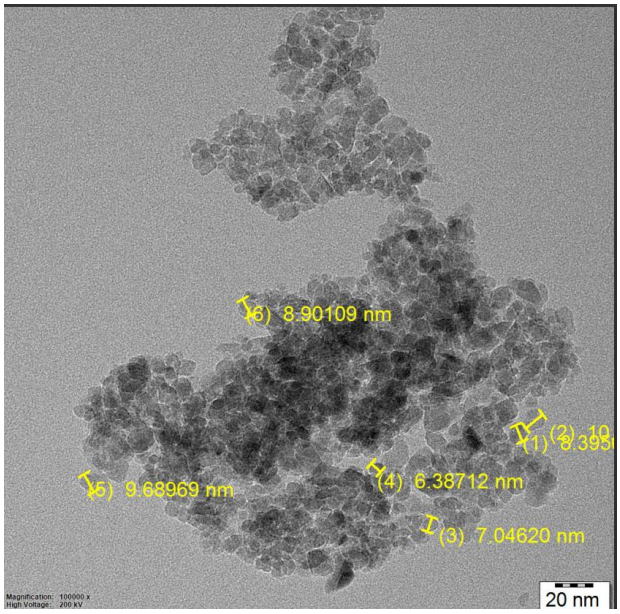

Fig. 8. TEM image of TiO_2.

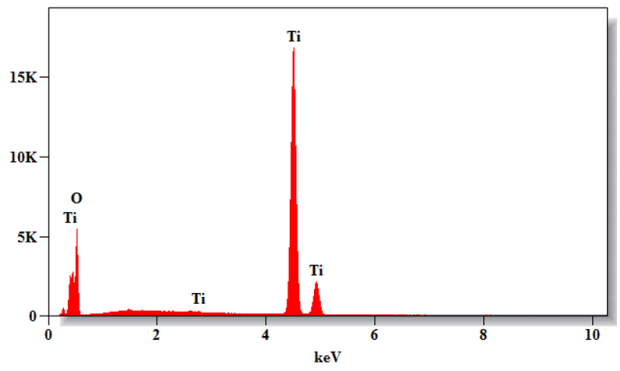

Fig. 9. Energy-dispersive X-ray spectroscopy (EDS).

The high intensity of these peaks indicates a strong presence of both elements, consistent with the expected composition of TiO_2. The spectrum also suggests the sample's purity, as no other elemental peaks are prominent. This analysis verifies the chemical composition of the TiO_2 nanoparticles, supporting their potential application in areas such as photocatalysis and nanotechnology.

Surfactants reduce surface tension, enabling better spreading, wetting, and dispersion in liquids. Used in detergents, emulsions, and textile dyeing, they prevent sedimentation and enhance particle dispersion. Sorbitan Monooleate (Span 80) is a biodegradable, non-ionic surfactant derived from oleic acid and sorbitol. It is effective in creating oil-in-water emulsions, especially with Tween 80, and is widely used in soaps, detergents, and particle dispersion. Span 80 is pale yellow, insoluble in water, but soluble in alcohol and organic solvents, with a molecular formula of $C_{24}H_{44}O_6$.

The formulation of nano lubricants involves the integration of nanoparticles SiO_2, Al_2O_3, and TiO_2 into a base oil SAE 10W-30, along with the use of a surfactant Span 80, to ensure stable dispersion. The chosen nano-additives are mixed with the SAE 10W-30 oil in three distinct ratios of 0.05%, 0.5%, and 1%. The particle sizes for SiO_2, Al_2O_3, and TiO_2 are 89 nm, 111.5 nm, and 18 nm respectively.

3. RESULTS AND DISCISSION

Taguchi's statistical method was employed to analyse all parameters using a limited number of experiments. This method utilizes the signal-to-noise (S/N) ratio to measure how closely quality characteristics align with or deviate from ideal values [6]. In this study, nanoparticles such as SiO_2, Al_2O_3, and TiO_2 were considered. The L27 Taguchi orthogonal array [7] was selected to accommodate three parameters at three levels, following Taguchi's experimental design principles [8]. Table 3 summarizes the factors and their corresponding levels. When analysing the S/N ratio, three quality categories are considered: "lower is better," "higher is better," and "nominal is best." This method not only determines the main effects of each factor but also identifies their interactions on the response variable, such as the lubricant's performance metrics. A three-level factorial design is employed, where each factor is evaluated at three levels: low, intermediate, and high.

Table 3. The independent levels of variables.

Input variables (nanoparticles)	Level of variable (wt. %)		
	1	2	3
SiO_2	0.05	0.5	1
TiO_2	0.05	0.5	1
Al_2O_3	0.05	0.5	1

In this study, three additives (SiO_2, Al_2O_3, and TiO_2) were selected, each tested at three distinct concentration levels (0.05%, 0.5%, and 1%). This design yields 27 unique samples or treatments, covering all possible combinations of factors and levels [9-11]. In this study, the optimal values for the resultant features such as SWR, CoF, density, and kinematic viscosity were determined using the "smaller is better" criterion. For thermal properties like flash point and fire point, the "larger is better" criterion was applied. The Taguchi method was employed to optimize the process parameters, while analysis of variance (ANOVA) was used to evaluate and quantify the contribution of each parameter.

To prepare the nanofluid, the base oil and nanoparticle mixture was first stirred for 30 minutes at 300 RPM and 100°C using a hot plate magnetic stirrer, ensuring preliminary dispersion of the nanoparticles in the oil. Subsequently, the mixture underwent ultrasonic treatment in a cleaner for an additional 30 minutes at 60°C to further enhance the dispersion and stability of the nanoparticles within the base oil This comprehensive preparation method, combined with a structured experimental design, ensures a thorough investigation of the effects of nano-additives on the properties of SAE 10W-30 base oil. By evaluating 27 unique formulations, the study aims to identify the optimal concentration and combination of nanoparticles to enhance the lubricant's performance, including improved wear resistance, reduced friction, and enhanced thermal stability. This methodical approach to experimentation and analysis supports the development of high-performance nano-lubricants tailored to specific applications.

Most tribometer test applications assess wear by comparing the mass or surface characteristics of test objects before and after testing. In a pin-on-disc tribology test, with a pin diameter of 8 mm and an EN 31 steel disc, running at 600 rpm with a 30 mm sliding track radius for 300 seconds, measure initial and final pin weights to assess wear. A total of 27 samples were tested using the pin-on-disc apparatus following ASTM G99 standards, with the SWR and CoF results presented in Table 4.

From Table 4, Sample 26 exhibits the maximum SWR of 0.0043842 mm^3/Nm, while Sample 19 exhibits the minimum SWR of 0.0000382 mm^3/Nm. SWR is a crucial parameter in tribological studies, indicating the volume of material worn per unit load and distance. Lower SWR values suggest better wear resistance, while higher values indicate greater material loss under similar conditions.

Table 4. Average SWR and CoF values for 27 samples.

Sample No.	(Wt. %)			Specific Wear rate mm^3/Nm	CoF
	SiO_2	TiO_2	Al_2O_3		
Sample	0.05	0.05	0.05	0.001534	0.257
Sample	0.05	0.5	0.05	0.000392	0.185
Sample	0.05	1	0.05	0.000978	0.206
Sample	0.05	0.05	0.5	0.000144	0.003
Sample	0.05	0.5	0.5	0.000442	0.140
Sample	0.05	1	0.5	0.000682	0.188
Sample	0.05	0.05	1	0.000145	0.155
Sample	0.05	0.5	1	0.000256	0.120
Sample	0.05	1	1	0.000458	0.040
Sample	0.5	0.05	0.05	0.000285	0.132
Sample	0.5	0.5	0.05	0.000244	0.280
Sample	0.5	1	0.05	0.000315	0.133
Sample	0.5	0.05	0.5	0.000234	0.014
Sample	0.5	0.5	0.5	0.000166	0.080
Sample	0.5	1	0.5	0.000144	0.003
Sample	0.5	0.05	1	0.000298	0.060
Sample	0.5	0.5	1	0.000251	0.268
Sample	0.5	1	1	0.000276	0.124
Sample	1	0.05	0.05	0.000038	0.139
Sample	1	0.5	0.05	0.000080	0.150
Sample	1	1	0.05	0.000251	0.268
Sample	1	0.05	0.5	0.001049	0.300
Sample	1	0.5	0.5	0.000240	0.170
Sample	1	1	0.5	0.001049	0.300
Sample	1	0.05	1	0.000276	0.124
Sample	1	0.5	1	0.004384	0.374
Sample	1	1	1	0.000315	0.133

The data reveals variation across samples, with some exhibiting significantly lower SWR, demonstrating higher durability and wear resistance. Notable observations include sample 19, which have the lowest SWR values, suggesting their superior performance in reducing wear.

The Taguchi approach is an effective tool for designing experiments that allows for controlled data collection, analysis of the impact of process factors on specific outcomes, and development of

high-quality systems. In this research, the experimental results were analysed using the signal-to-noise (S/N) ratio as per the Taguchi method. For quality characteristics such as SWR, CoF, density, and kinematic viscosity, the "smaller-the-better" criterion was applied. Conversely, for thermal properties like flash point and fire point temperatures, the "higher-the-better" criterion was utilized. S/N analysis was conducted to calculate the S/N ratio for each level of the process parameters. Additionally, statistical analysis of variance (ANOVA) was performed to identify the statistically significant parameters and predict the optimal combination of test parameters. The S/N ratio for SWR, CoF, density, and kinematic viscosity was determined based on Taguchi's "smaller-the-better" approach.

$$S/N = -10 \log [1/n (y_1^2 + y_2^2 + \ldots + y_n^2 \quad (1)$$

The S/N ratio for flash point and fire point was determined based on Taguchi's "larger-the-better" criterion.

$$S/N = -10 \log [1/n (1/y_1^2 + 1/y_2^2 + \ldots + 1/y_n^2)], \quad (2)$$

Here y_1, y_2, …, yn represent the responses for SWR, CoF, density, kinematic viscosity, flash point, and fire point, where n is the number of observations. Minitab software was utilized to generate mean-response graphs, and ANOVA was performed to determine the percentage contribution of each testing parameter. Figure 10 illustrates the normal probability plots of residuals for the predicted SWR response. The regression coefficient (R^2 = 0.828) aligns well with the adjusted regression coefficient (R^2adj =0.768), indicating a good fit for the model.

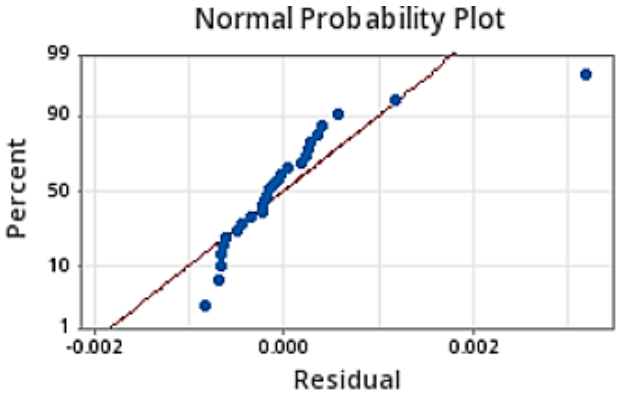

Fig. 10. Normal probability plots for SWR point.

Table 5 shows that SiO_2 has the highest statistical impact on SWR, contributing 9%, followed by Al_2O_3 at 2.55%. In contrast, TiO_2 exhibits the least effect on SWR.

Table 5. Analysis of SWR variance through ANOVA.

Source	DF	Adj SS	Contribution (%)	Adj MS	F-Value	P-Value
SiO_2	2	0.000001663	9.00	0.000001	1.041	0.371
TiO_2	2	0.0000003771	2.04	0.000000	0.236	0.792
Al_2O_3	2	0.0000004727	2.55	0.000000	0.296	0.747
Error	20	0.00001597	86.41	0.000001		
Total	26	0.00001848	100			

The results indicate that the addition of SiO_2 nanoparticles can effectively improve the SWR of frictional components. Figure 11 presents the average response values and S/N ratios for SWR, highlighting the principal effects of the optimal parameters on SWR. In the ANOVA analysis, the percentage contribution quantifies the impact of process parameters on the output response. The p-value is used to assess the significance of process variables, with values below 0.05 indicating statistical insignificance [12]. The F-value serves as a statistical tool to identify design factors that significantly influence the quality characteristics [13]. Higher signal-to-noise (S/N) ratios correspond to improved efficiency [14].

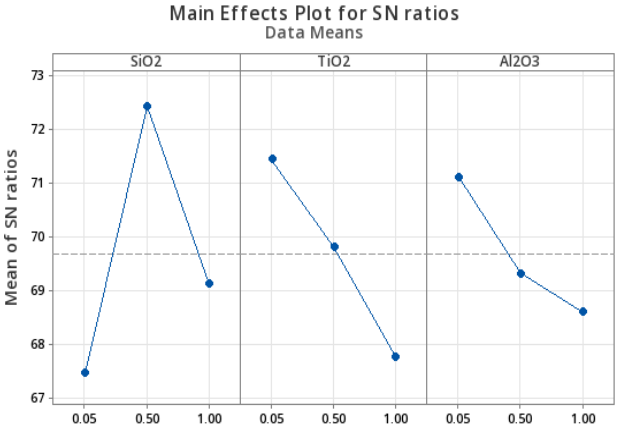

Fig. 11. Main effect tribological parameter on SWR.

The optimal SWR is achieved at X1 level 2, X2 level 1, and X3 level 1 as shown in Figure 11. The most effective parameters, based on the highest S/N ratio for SWR, are 0.5 wt.% SiO_2, 0.05 wt.% TiO_2, and 0.05 wt.% Al_2O_3. This optimum combination (0.5,0.05,0.05) represents the best configuration for minimizing SWR.

According to Table 4, Sample 26 exhibits the maximum CoF value of 0.3742, whereas Sample 4 and Sample 15 demonstrate the minimum CoF value of 0.003. CoF is a critical parameter in friction studies, as it measures the resistance to sliding between two contacting surfaces. Lower CoF values indicate better sliding performance of mating parts, while higher values reflect greater frictional losses under similar conditions. The data shows variation across samples, with some demonstrating significantly lower CoF values, suggesting better durability and smoother operation. Notable examples are Samples 4 and 15, which exhibit the lowest CoF values, indicating their superior performance in reducing friction.

Figure 12 presents normal probability plots of residuals for the predicted CoF responses. The regression coefficient R^2 (0.828) is in good agreement with the adjusted regression coefficient R^2adj (0.768).

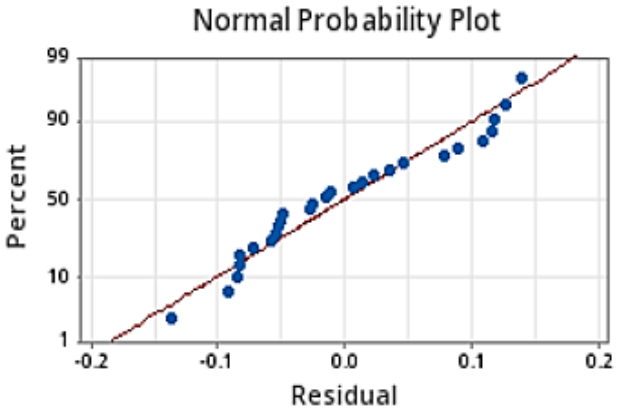

Fig. 12. Normal probability plots for CoF

Table 6 reveals that SiO_2 has the greatest statistical impact on CoF at 18.53 %, followed by TiO_2 at 7.94 %, meanwhile, Al_2O_3 has the smallest effect on CoF. The ANOVA table analyzes the effects of SiO_2, TiO_2, and Al_2O_3 on the total variance in the response variable. SiO_2 has the most significant impact among the factors, with an F-value of 2.791 and a P-value of 0.085, contributing 18.53% to the total variance.

Table 6. Analysis of CoF variance through ANOVA

Source	DF	Adj SS	Contribution (%)	Adj MS	F-Value	P-Value
SiO_2	2	0.04535	18.53	0.022675	2.791	0.085
TiO_2	2	0.01943	7.94	0.009717	1.196	0.323
Al_2O_3	2	0.01751	7.15	0.008756	1.078	0.359
Error	20	0.16248	66.38	0.008124		
Total	26	0.24478	100			

While SiO_2's effect is not statistically significant at the 0.05 level, it approaches significance, indicating a moderate influence on the response variable. TiO_2 and Al_2O_3 have minimal effects, contributing 7.94% and 7.15% to the total variance, respectively, with high P-values (0.323 and 0.359), suggesting no significant impact. The error term accounts for the majority of the variability (66.38%), implying that much of the variation in the data is unexplained by the factors in the model. The total sum of squares for all sources is 0.24478, capturing the overall variation in the response variable across the factors. The optimal CoF is achieved at X1 level 2, X2 level 1, and X3 level 2 as shown in Figure 13.

The most effective parameters, based on the highest S/N ratio for CoF, are 0.5 wt.% SiO_2, 0.05 wt.% TiO_2, and 0.5 wt.% Al_2O_3. Thus, the optimal combination for minimizing CoF is 0.5,0.05,0.5.

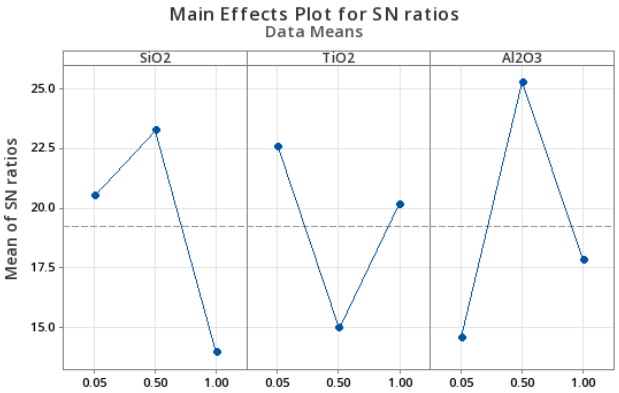

Fig. 13. Main effect tribological parameter on CoF.

The measurement of flash and fire points using the Cleveland open cup tester in accordance with ASTM D92 standards. The results are provided in Table 7. From Table 7, Sample 15 exhibits the maximum flashpoint value of 210.7℃, while Sample 26 exhibits the minimum flashpoint value of 190.5℃. Flash and fire point temperatures of oil are crucial for assessing safety and performance, as they indicate the oil's flammability and ability to sustain combustion under high-temperature conditions.

Figure 14 presents the normal probability plots of residuals for the predicted flash point responses. The regression coefficient R^2 (0.9381) aligns well with the adjusted regression coefficient R^2adj (0.7988).

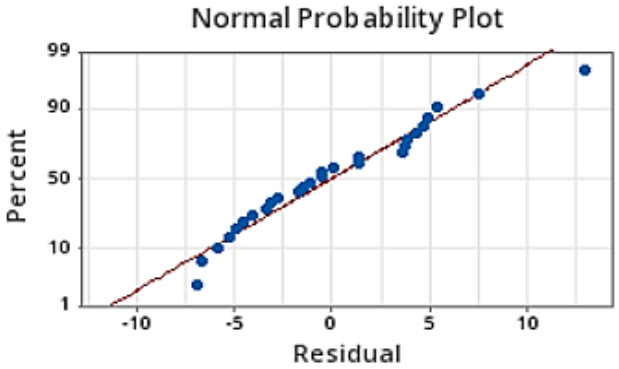

Fig. 14. Normal probability plots for flash point.

Table 8 shows that SiO_2 has the largest statistical impact on the flash point, contributing 23.78%, followed by TiO_2 at 5.61%. In contrast, Al_2O_3 has the smallest effect on the flash point.

Table 7. Flash and Fire points for 27 samples.

Sample No.	SiO_2 (wt.%)	TiO_2 (wt.%)	Al_2O_3 (wt.%)	Flash point in ℃	Fire point in ℃
Sample 01	0.05	0.05	0.05	197.1	205.3
Sample 02	0.05	0.5	0.05	194.5	220.0
Sample 03	0.05	1	0.05	204.9	220.0
Sample 04	0.05	0.05	0.5	196.9	210.0
Sample 05	0.05	0.5	0.5	202.5	217.6
Sample 06	0.05	1	0.5	195.5	224.6
Sample 07	0.05	0.05	1	198.6	214.0
Sample 08	0.05	0.5	1	209.0	220.4
Sample 09	0.05	1	1	192.0	215.0
Sample 10	0.5	0.05	0.05	207.0	226.0
Sample 11	0.5	0.5	0.05	195.6	207.0
Sample 12	0.5	1	0.05	201.0	227.0
Sample 13	0.5	0.05	0.5	208.0	222.0
Sample 14	0.5	0.5	0.5	193.7	213.0
Sample 15	0.5	1	0.5	210.7	225.5
Sample 16	0.5	0.05	1	202.0	212.0
Sample 17	0.5	0.5	1	193.0	209.0
Sample 18	0.5	1	1	205.0	219.0
Sample 19	1	0.05	0.05	200.2	215.0
Sample 20	1	0.5	0.05	198.7	210.4
Sample 21	1	1	0.05	190.6	205.9
Sample 22	1	0.05	0.5	196.3	204.5
Sample 23	1	0.5	0.5	192.6	205.5
Sample 24	1	1	0.5	197.7	222.0
Sample 25	1	0.05	1	192.0	210.0
Sample 26	1	0.5	1	190.5	210.0
Sample 27	1	1	1	196.0	209.0

Table 8. Analysis of Flash point variance through ANOVA.

Source	DF	Adj SS	Contribution (%)	Adj MS	F-Value	P-Value
SiO_2	2	211.85	23.78	105.924	3.45	0.052
TiO_2	2	49.96	5.61	24.981	0.814	0.457
Al_2O_3	2	14.83	1.67	7.414	0.241	0.788
Error	20	614.11	68.94	30.705		
Total	26	890.75	100			

The ANOVA table shows SiO_2 significantly impacts the response variable (F = 3.45, P = 0.052), contributing 23.78 % to total variation. TiO_2 (5.61%, P = 0.457) and Al_2O_3 (1.67%, P = 0.788) have minimal and insignificant effects. The error term accounts for 68.94% of variability, indicating factors outside the model dominate the response, with a total sum of squares of 890.75. The results indicate that the addition of SiO_2 nanoparticles may enhance the flash point. Figure 15 shows the average response values and S/N ratios for the flash point, presenting the principal results of the optimal parameters for improving the flash point.

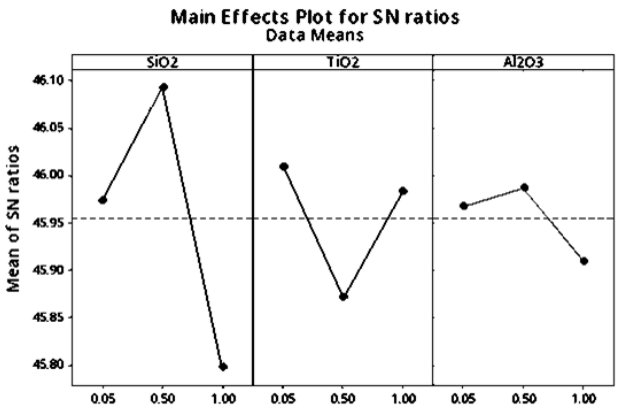

Fig. 15. Normal probability plots for flash point.

The optimal flash point is achieved at X1 level 2, X2 level 1, and X3 level 2 as shown in Figure 15. The most effective parameters, based on the highest S/N ratio for flash point, are 0.5 wt.% SiO_2, 0.05 wt.% TiO_2, and 0.5 wt.% Al_2O_3.

From Table 7, Sample 12 also shows the maximum fire point value of 227˚C, whereas Sample 22 has the minimum fire point value of 204.5˚C. Figure 16 shows the normal probability plots of residuals for the predicted fire point responses. The regression coefficient R^2 (0.999) aligns well with the adjusted regression coefficient R_2adj (0.999).

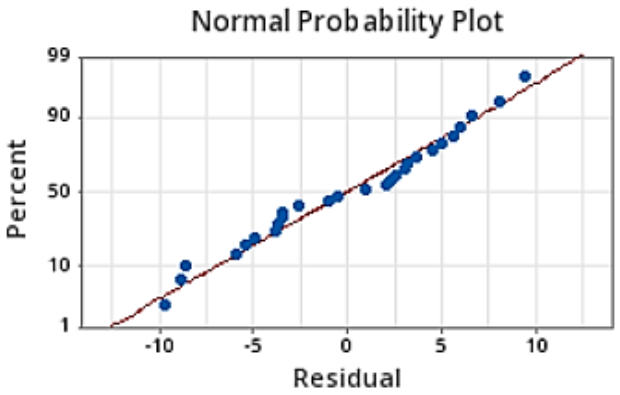

Fig. 16. Normal probability plots for fire point.

Table 9 shows that SiO_2 has the largest statistical impact on the fire point, contributing 22.447%, followed by TiO_2 at 15.769%. In contrast, Al_2O_3 has the smallest effect on the fire point.

Table 9. Analysis of Fire point variance through ANOVA

Source	DF	Adj SS	Contribution (%)	Adj MS	F-Value	P-Value
SiO_2	2	289.53	22.447	144.77	3.83	0.039
TiO_2	2	203.39	15.769	101.69	2.69	0.092
Al_2O_3	2	40.32	3.126	20.16	0.53	0.595
Error	20	756.61	58.658	37.83		
Total	26	1289.85	100			

The ANOVA table assesses the contributions of three factors SiO_2, TiO_2, and Al_2O_3 to the total variance in the response variable. SiO_2 exhibits a significant effect with an F-value of 3.83 and a P-value of 0.039, contributing 22.45% to the total variation, indicating its meaningful impact on the response. TiO_2, with an F-value of 2.69 and a P-value of 0.092, contributes 15.77%, but its effect is not statistically significant ($p > 0.05$). Al_2O_3 contributes minimally, at 3.13%, and has a high P-value of 0.595, indicating it does not significantly influence the response variable. The error term, which accounts for 58.66% of the total variance, suggests that more than half of the variability in the data is due to factors not included in the model. The total sum of squares across all sources is 1289.85, representing the complete variation in the response variable across the factors. The results indicate that the addition of SiO_2 nanoparticles can enhance the fire point. The average response values and S/N ratio for fire point are shown in Figure 17, which presents the principal results of the optimal parameters for the fire point.

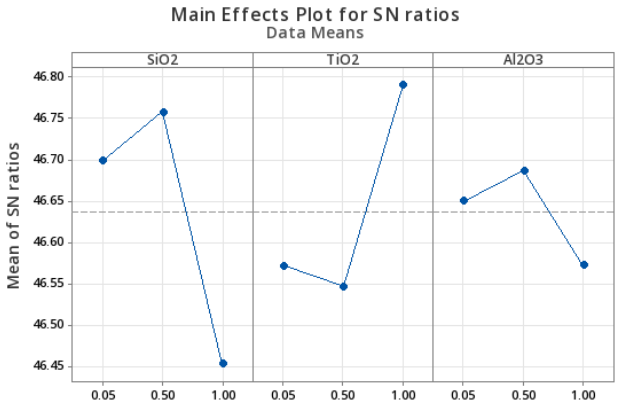

Fig. 17. Normal probability plots for fire point.

The optimal fire point is achieved at X1 level 2, X2 level 3, and X3 level 2, as shown in Figure 17. The most effective parameters, based on the highest S/N ratio for fire point, are 0.5 wt.% SiO_2, 1 wt.% TiO_2, and 0.5 wt.% Al_2O_3. The optimal combination for achieving the best fire point is 0.5, 1, 0.5.

Using Saybolt universal viscosity test, the kinematic viscosity of a sample nanofluid was measured in accordance with ASTM D88 standards by measuring the time it takes for a specific volume of

the fluid to pass through a calibrated tube at a constant temperature. For this test, the sample nanofluid is first heated to the test temperature of 55°C to ensure consistency in the viscosity measurement [15]. Once the sample reaches the desired temperature, it is poured into the Saybolt viscometer apparatus. The calibrated tube is then filled with the heated nanofluid, and the timer is started as soon as the fluid starts flowing. The time duration for 60 ml of the nanofluid to pass through the tube is given in Table 13 for 27 samples. The time measurement is crucial as it directly correlates with the viscosity of the nanofluid. The kinematic viscosity of the nanofluid is calculated using the recorded time duration and the specifications of the Saybolt viscometer apparatus. This test provides valuable information about the flow characteristics and viscosity behaviour of the nanofluid at the specified temperature, aiding in various industrial and research applications where viscosity control is essential. From Table 10, Sample 6 exhibits the maximum density value of 0.993 g/ml, while Sample14 exhibits the minimum density value of 0.923 g/ml.

Figure 18 illustrates the normal probability diagrams of residuals for the predicted responses for the fire point. The regression coefficient R^2 (1.000) aligns well with the adjusted regression coefficient R^2 (0.999), indicating an excellent fit of the model to the data.

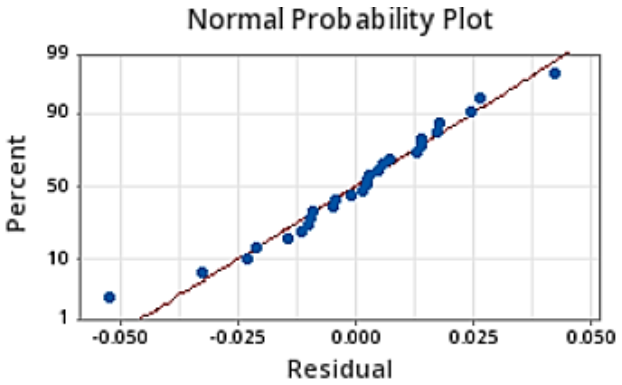

Fig. 18. Normal probability plots for density

Table 10. Density and Kinematic viscosity values for 27 samples.

Sample No.	SiO_2 (wt.%)	TiO_2 (wt.%)	Al_2O_3 (wt.%)	Density (g/ml)	Kinematic viscosity @55°C (m2/s)
Sample 01	0.05	0.05	0.05	0.904	29.347
Sample 02	0.05	0.5	0.05	0.958	14.798
Sample 03	0.05	1	0.05	0.987	14.266
Sample 04	0.05	0.05	0.5	0.964	14.529
Sample 05	0.05	0.5	0.5	0.938	29.349
Sample 06	0.05	1	0.5	0.993	14.53
Sample 07	0.05	0.05	1	0.942	14.639
Sample 08	0.05	0.5	1	0.975	14.529
Sample 09	0.05	1	1	0.932	14.266
Sample 10	0.5	0.05	0.05	0.973	16.361
Sample 11	0.5	0.5	0.05	0.967	14.266
Sample 12	0.5	1	0.05	0.966	15.318
Sample 13	0.5	0.05	0.5	0.956	30.879
Sample 14	0.5	0.5	0.5	0.923	17.916
Sample 15	0.5	1	0.5	0.945	14.267
Sample 16	0.5	0.05	1	0.962	20.230
Sample 17	0.5	0.5	1	0.985	15.318
Sample 18	0.5	1	1	0.947	14.798
Sample 19	1	0.05	0.05	0.986	14.825
Sample 20	1	0.5	0.05	0.973	14.798
Sample 21	1	1	0.05	0.981	15.055
Sample 22	1	0.05	0.5	0.965	15.055
Sample 23	1	0.5	0.5	0.967	14.53
Sample 24	1	1	0.5	0.956	15.055
Sample 25	1	0.05	1	0.97	29.099
Sample 26	1	0.5	1	0.987	14.529
Sample 27	1	1	1	0.95	22.282

Table 11 reveals that SiO_2 has the greatest statistical impact on density at 10.57 %, followed by Al_2O_3 at 3.67 %, meanwhile, TiO_2 has the smallest effect on density. The ANOVA table provides a statistical analysis of the effects of three factors are SiO_2, TiO_2, and Al_2O_3 on a response variable.

Table 11. Analysis of density variance through ANOVA.

Source	DF	Adj SS	Contribution (%)	Adj MS	F-Value	P-Value
SiO_2	2	0.001239	10.57	0.000619	1.251	0.308
TiO_2	2	0.000151	1.29	0.000076	0.153	0.859
Al_2O_3	2	0.000430	3.67	0.000215	0.435	0.653
Error	20	0.009900	84.47	0.000495		
Total	26	0.011720	100			

The table breaks down the sources of variation and presents details on degrees of freedom (DF), adjusted sums of squares (Adj SS), adjusted mean squares (Adj MS), F-values, P-values, and percentage contributions. The factor SiO_2 has an F-value of 1.251 and a P-value of 0.308, contributing 10.57% to the total variance, which is higher than the other factors but not statistically significant ($p > 0.05$). TiO_2 and Al_2O_3 have minimal contributions of 1.29% and 3.67%, respectively, with high P-values, indicating they have negligible effects on the response. The error term accounts for most of the variance (84.47%), suggesting that much of the variability in the data is due to unexplained factors not included in this model. The total sum of squares for all sources is 0.011720, representing the complete variation in the response variable across all factors. The results indicate that the addition of SiO_2 nanoparticles can be utilized to enhance density. Figure 19 presents the average response values and S/N ratios for density, illustrating the principal outcomes of the optimal parameters.

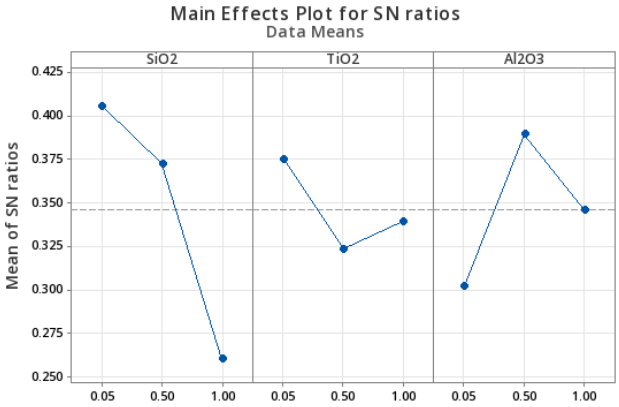

Fig. 19. Normal probability plots for density.

The optimal density is achieved at X1 Level 1, X2 Level 1, and X3 Level 2, as shown in Figure 19. The most effective parameters, based on the highest S/N ratio for density, are 0.05 wt.% SiO_2, 0.05 wt.% TiO_2, and 0.5 wt.% Al_2O_3. The optimal combination of levels (0.05, 0.05, 0.5) is also ideal for attaining the maximum density.

Table 10 reveals that Sample 13 shows the maximum Kinematic viscosity value of 30.879 m2/s, whereas Sample 3,9 and 11 has the minimum Kinematic viscosity value of 14.266 m2/s. Figure 20 presents the normal probability diagrams of residuals for the predicted responses of kinematic viscosity. The regression coefficient R^2 (0.931) aligns well with the adjusted regression coefficient R^2 (0.906), indicating a strong model fit.

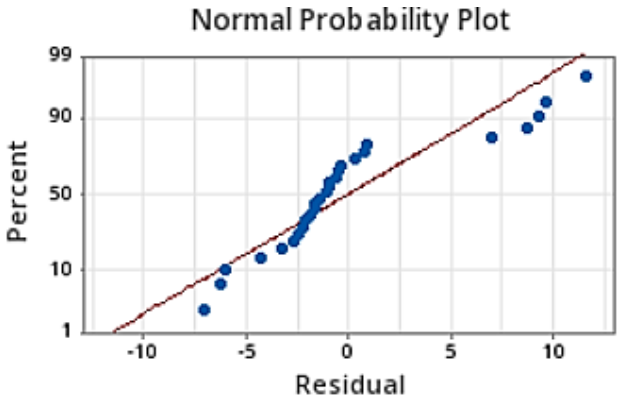

Fig. 20. Normal probability plots for kinematic viscosity

Table 12 reveals that TiO_2 has the greatest statistical impact on kinematic viscosity at 16.03 %, followed by Al_2O_3 at 2.13 %, meanwhile, TiO_2 has the smallest effect on kinematic viscosity. In this ANOVA table, we analyse the effects of three factors SiO_2, TiO_2, and Al_2O_3 on an outcome variable to determine if they have statistically significant impacts. Each factor is evaluated with DF of 2, indicating they each have three levels. The "Error" row captures the unexplained variation, with 20 DF, while the total DF for the analysis is 26.

Table 12. Analysis of Kinematic viscosity variance through ANOVA.

Source	DF	Adj SS	Contribution (%)	Adj MS	F-Value	P-Value
SiO_2	2	1.596	0.21	0.7979	0.03	0.975
TiO_2	2	124.474	16.03	62.2372	1.96	0.167
Al_2O_3	2	16.529	2.13	8.2647	0.26	0.773
Error	20	633.945	81.64	31.6972		
Total	26	776.545	100			

The F-Value for each factor is calculated by dividing the Adj MS of the factor by the Adj MS of the error, providing a test statistic to assess significance. However, with P-values of 0.975 for SiO_2, 0.167 for TiO_2, and 0.773 for Al_2O_3, none of these factors exhibit statistical significance at the typical threshold of 0.05. This suggests that variations in SiO_2, TiO_2, and Al_2O_3 do not significantly affect the outcome, as supported by the relatively low F-values and high P-values.

The results indicate that the addition of TiO_2 nanoparticles can effectively enhance the kinematic viscosity. Figure 21 illustrates the average response values and S/N ratios, highlighting the principal outcomes of the optimal parameters for kinematic viscosity. The optimal kinematic viscosity is achieved at X1 Level 3, X2 Level 3, and X3 Level 1, as shown in Figure 21. The most influential parameters, based on the highest S/N ratio for kinematic viscosity, are 1 wt.% SiO_2, 1 wt.% TiO_2, and 0.05 wt.% Al_2O_3. Thus, the optimal combination for attaining maximum kinematic viscosity is (1, 1, 0.05).

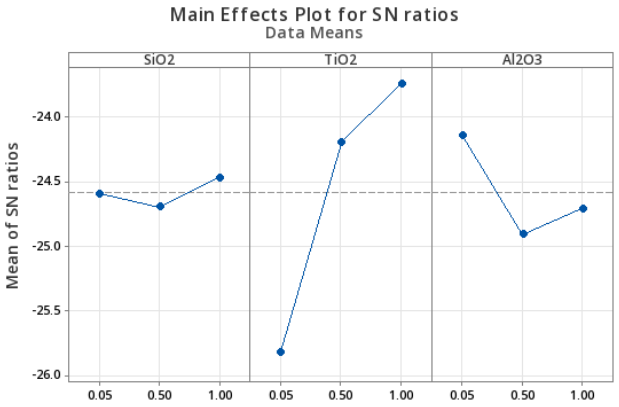

Fig. 21. Normal probability plots for kinematic viscosity.

Table 13 presents the optimal mix ratios of SiO_2, TiO_2, and Al_2O_3 additives with base oil, determined through Taguchi analysis, to achieve the best performance for each measured property. Table 13 shows the results from Taguchi analysis applied to a multi-objective polynomial equation helped in identifying the optimal blend of nanoparticles for a high-performance lubricant. The analysis determined that the ideal mix consists of 0.05 wt.% of SiO_2, 1 wt.% of TiO_2, and 0.3 wt.% of Al_2O_3.

Table 13. Taguchi optimal values for each property.

SiO_2	TiO_2	Al_2O_3	Specific wear rate (mm^3/Nm)	CoF	Density (g/ml)	Flash point ˚C	Fire point ˚C	Kinematic viscosity (m^2/s)	Optimal property
0.5	0.05	0.05	0.000285	0.1327	0.973	207	226	16.3614	SWR
0.5	0.05	0.5	0.000234	0.014	0.956	208	222	30.879	CoF
0.05	0.05	0.5	0.000144	0.003	0.964	196.9	210	14.529	Density
0.5	0.05	0.5	0.000234	0.014	0.956	208	222	30.879	Flash point
0.5	1	0.5	0.000144	0.003	0.945	210.7	225.5	14.267	Fire point
1	1	0.05	0.0002515	0.2685	0.981	190.6	205.9	15.055	KV

4. CONCLUSION

The focus in this research was on the development and characterization of advanced lubricant formulations by incorporating various nanoparticles and surfactants to improve the performance of SAE10W30 base oils. This research involved the formulation and analysis of 27 different nonadditive-infused base oil samples, with varying concentrations and combinations of SiO2, Al_2O_3, and TiO_2 nanoparticles. The research then proceeded with a series of experimental investigations to assess the tribological, thermal, and rheological properties of the formulated lubricants. The Taguchi method allowed for systematic experimentation to identify the most influential factors on performance, while ANOVA helped quantify the significance of each parameter and their interactions. Studies have shown that varying the weight percentages of SiO_2, TiO_2, and Al_2O_3 can significantly impact the overall performance of nano-lubricants. A multi-objective polynomial equation helped in identifying the optimal blend of nanoparticles for a high-performance lubricant. The analysis determined that the ideal mix consists of 0.05 wt.% of SiO_2, 1 wt.% of TiO_2, and 0.3 wt.% of Al_2O_3.

REFERENCES

[1] N. Desai, A. M. Nagaraj, and N. Sabnis, "Analysis of thermo-physical properties of SAE20W40 engine oil by the addition of SiO2 nanoparticles," *Mater. Today: Proc.*, vol. 47, pp. 5646–5651, 2021, doi: 10.1016/j.matpr.2021.03.688.

[2] D. Peng, C. Chen, Y. Kang, Y. Chang, and S. Chang, "Size effects of SiO2 nanoparticles as oil additives on tribology of lubricant," *Ind. Lubr. Tribol.*, vol. 62, no. 2, pp. 111–120, 2010, doi: 10.1108/00368791011025656.

[3] H. H. Patil and D. Sangli, "Tribological properties of SiO2 nanoparticles added in SN-500 base oil," *Int. J. Eng. Res. Technol.*, vol. 2, no. 5, pp. 763–788, 2013.

[4] H. Li, S. Li, F. Li, Z. Li, and H. Wang, "Fabrication of SiO2 wrapped polystyrene microcapsules by Pickering polymerization for self-lubricating coatings," *J. Colloid Interface Sci.*, vol. 528, pp. 92–99, 2018, doi: 10.1016/j.jcis.2018.05.081.

[5] Y. S. Dambatta et al., "Tribological performance of SiO2-based nanofluids in minimum quantity lubrication grinding of Si3N4 ceramic," *J. Manuf. Process.*, vol. 1, no. 4, pp. 135–147, 2019, doi: 10.1016/j.jmapro.2019.03.024.

[6] T. Goyal, R. S. Walia, and T. S. Sidhu, "Study of coating thickness of cold spray process using Taguchi method," *Mater. Manuf. Process.*, vol. 27, no. 2, pp. 185–192, 2012, doi: 10.1080/10426914.2011.564249.

[7] K. Hashmi, I. D. Graham, and B. Mills, "Fuzzy logic based data selection for the drilling process," *J. Mater. Process. Technol.*, vol. 108, no. 1, pp. 55–61, 2000, doi: 10.1016/S0924-0136(00)00597-5.

[8] M. Aamir, S. Tu, M. Tolouei-Rad, K. Giasin, and A. Vafadar, "Optimization and modeling of process parameters in multi-hole simultaneous drilling using Taguchi method and fuzzy logic approach," *Materials*, vol. 13, no. 3, p. 680, 2020, doi: 10.3390/ma13030680.

[9] E. Sankar and K. Duraivelu, "Evaluation of some thermo-physical properties of SN500 lubrication oil blended with SiO2, Al2O3, and TiO2 nano additives, using fuzzy logic," *Acta Mech. Autom.*, vol. 18, no. 2, pp. 352–360, 2024, doi: 10.2478/ama-2024-0039.

[10] E. Sankar and K. Duraivelu, "Simulation of optimal mix of SiO2, TiO2 and Al2O3, nano additives for the minimal wear and coefficient of friction of lubricant using fuzzy logic," *J. Teknol.-Sci. Eng.*, vol. 86, no. 1, pp. 125–133, 2024, doi: 10.11113/jurnalteknologi.v86.20402.

[11] E. Sankar and K. Duraivelu, "The effect of SiO2, Al2O3, and TiO2 nanoparticle additives on lubrication performance: Evaluation of wear and coefficient of friction," *Mater. Today: Proc.*, vol. 68, no. 6, pp. 2387–2392, 2022, doi: 10.1016/j.matpr.2022.09.107.

[12] A. Zerti et al., "Prediction of machining performance using RSM and ANN models in hard turning of martensitic stainless steel AISI 420," *Proc. Inst. Mech. Eng., Part C: J. Mech. Eng. Sci.*, vol. 233, no. 13, pp. 4439–4462, 2019, doi: 10.1177/0954406218820557.

[13] M. Kurt, E. Bagci, and Y. Kaynak, "Application of Taguchi methods in the optimization of cutting parameters for surface finish and hole diameter accuracy in dry drilling processes," *Int. J. Adv. Manuf. Technol.*, vol. 40, pp. 458–469, 2019, doi: 10.1007/s00170-007-1368-2.

[14] W. P. Yang and Y. S. Tarng, "Design optimization of cutting parameters for turning operations based on the Taguchi method," *J. Mater. Process. Technol.*, vol. 84, no. 3, pp. 122–129, 1998, doi: 10.1016/S0924-0136(98)00079-X.

[15] S. B. Mousavi, S. Z. Heris, and P. Estellé, "Viscosity, tribological and physicochemical features of ZnO and MoS2 diesel oil-based nanofluids: An experimental study," *Fuel*, vol. 1, pp. 293–311, 2021, doi: 10.1016/j.fuel.2021.120481.